Neural Network-Aided Spurious Modes Optimization Targeting Lithium Niobate MEMS Resonators

Luca Colombo[1], Luca Baldesi[1], Tommaso Melodia[1], Gianluca Piazza[2], and Matteo Rinaldi[1]
[1]Department of Electrical and Computer Engineering, Northeastern University, Boston MA, USA
[2]Department of Electrical and Computer Engineering, Carnegie Mellon University, Pittsburgh PA, USA
[1] l.colombo@northeastern.edu

***Abstract*— This work reports on the implementation of a neural network (NN) feature selection approach to identify the design features that impact the rise of spurious modes in high performance X-cut Lithium Niobate MEMS resonators. A metric based on spurious modes location, number, and peak-to-peak excursion is introduced to serve as a target function for the NN training. Measured data from 814 fabricated resonators operating between 50 MHz and 1 GHz is used to train and validate the NN and identify the most significant design features that introduce spurious responses. Number of electrode pairs, electrode length, and anchor width are found to be the driving feature of this process. To verify the NN outcome, finite element simulations based on optimized and non-optimized feature sets are finally reported, showing significant spurious modes suppression.**

***Keywords*— MEMS, Neural Network, Machine Learning, Lithium Niobate, Resonators**

I. Introduction

Envisioned Internet of Things (IoT) and 5G applications, including ultra-low-power or zero-energy wake-up receivers (WuRx) and tunable, reconfigurable filter banks are driving the demand for radio frequency (RF), microacoustic electromechanical systems (MEMS) with enhanced performance compared to state-of-the-art demonstrated devices [1][2]. Key-enabler device properties for the aforementioned applications include, but are not limited to, high quality factor at resonance (Q_s), high electromechanical coupling (k_t^2), spurious-free response in the frequency range of implementation, and impedance matching between the resonator static capacitance (C_0) and the given port termination [3]. Different technologies have been investigated in recent years to achieve the desired properties altogether and outperform commercially available Bulk Acoustic Wave (BAW) and Surface Acoustic Wave (SAW) resonators [4]. The most interesting demonstration include Aluminum Nitride (AlN) and Scandium-doped Aluminum Nitride (ScAlN) Contour Mode Resonators (CMRs) [5][6], Cross-sectional Lamé Mode Resonators (CLMRs) [7], Lead-zirconate Titanate (PZT) [8], quartz [9], and thin-film, single crystal Lithium Niobate (LN) resonators [10][11][12]. Among this last class of acoustic devices, recently developed LN S0 mode Laterally Vibrating Resonators (LVRs) have showcased unprecedent quality factors (up to 10,000 in vacuum) while retaining large electromechanical coupling (k_t^2>30%) at very and ultra-high frequency (VHF/UHF), gathering research interest for novel Internet of Things and 5G applications [13]. However, the combination of low intrinsic material losses and large available piezoelectric coefficients make touhis technology susceptible to unwanted in-band spurious modes that are detrimental for most of the envisioned applications [14]. For this reason, their control and optimization is still of research interest for a future commercialization of this technology.

In parallel with conventional spurious modes suppression techniques based on analytical modeling [15] and finite element analysis (FEA) [16], machine-learning techniques can also be used to rank features by contribution to spurious modes, hence guiding practitioners in their design. In particular, Deep Feature Selection (DFS) [17] is a neural network framework meant to identify the most relevant features for a given application. It has already been successfully applied in genomics [17], socio-economics [18], and Lithium-Ion Battery modeling [19]. In this paper, we design and test a Neural Network (NN) applying DFS to identify the main design factors that impact the rise of spurious modes in conventional, state-of-the-art high performance LVRs.

In the first section of this work, the resonators targeted by this investigation are briefly described, and a metric (M) to quantify the severity of spurious modes is introduced. In the second section, details on the DFS NN design and implementation are reported. Finally, in the third and last section, experimental results are discussed and validated via a Finite Element Analysis (FEA) approach.

II. Lithium Niobate Resonators

A. Topology and Characterization

Top-electrode only, Laterally Vibrating Resonators (LVRs) operating in the S_0 mode are fabricated on 1 and 2 um (h) thin film X-cut 30° YZ Lithium Niobate (LN) [3] on high resistivity silicon. The resonators topology consists in a suspended rectangular plate on which interdigitated electrodes (IDEs) are spaced by half wavelength (λ) to generate a standing acoustic wave that is transduced from the input to the output terminals. The main geometrical features of the resonators' design are highlighted in Fig. 1, while their implemented variations in Table 1. SEM of fabricated devices between 100 MHz and 1 GHz are reported in Fig. 2 together with the adopted fabrication process. After devices' release, the admittance response (Y) of 814 unique LVRs fabricated on different chips is recorded by direct wafer probing on fabricated devices operating between 50 MHz and 1 GHz (Fig. 2) in laboratory conditions. An example of measured Y_{12}

Table 1. Design parameters variations. Metal thickness (t_m) and anchor length (L_a) are fixed to 300 nm and 0.75 λ. In addition to the geometrical variations, devices' chip rows (R) and columns (C) are added as variables to take into account the effect of location on M.

Variable	Sym.	Value	#
Wavelength	λ	6 – 8 – 11 – 15 – 30 – 56 – 116 µm	8
LN thickness	h	1 - 2 µm	5
Aperture	L_e	3 – 5 – 7 – 9 – 11 – 13 λ	2
Bus length	L_b	0.25 – 0.75 – 1.75 – 2.25 – 2.75 – 3.25 – 4.25 – 4.75 – 5.25 – 5.75	7
Chip row	R	2 - 3	9
Anchor width	W_a	0.25 – 0.5 – 0.75 – 1 – 1.25 – 1.75 – 1.5 – 2 λ	3
Finger pairs	N_p	3 – 5 – 7 – 9 – 11	1
Coverage	c	0.1 – 0.2 – 0.3 – 0.5 – 0.8	10
Gap length	L_g	0.25 – 0.5 – 0.75 – 1.75 – 2.25 – 2.75 – 3.25 – 3.75 – 4.25 – 4.75 – 5.25 – 5.75 λ	4
Chip column	C	1 – 2 – 3	6

Table 2. Spurious metric (M) assessment criteria. M can vary between 0 (no spurious) and 7 (severe in-band spurious).

Factor	Criteria	Metric
Peak cleanness	Clean peak	+0
	Disturbed peak	+1
	Split peak	+2
Number of in-band spurious modes	0	+0
	1 - 2	+1
	2 - 4	+2
	>4	+3
Maximum spurious excursion (Δ_s)	<5 dB	+0
	>5 & <20 dB	+1
	>20 dB	+2

responses is reported in Fig. 3a. Due to the large, combined Q_s and k_t^2 attained, the devices present several in and out-of-band spurious modes, which are detrimental in many envisioned applications [14].

B. Spurious Metric (M) Definition

To quantitatively evaluate the presence and severity of in-band spurious modes and allow for algorithm-based optimization, a metric (M) is introduced. For each device, M is defined according to its Y response (Fig. 3a) and three factors: 1) peak cleanness; 2) number of in-band spurious modes; and 3) spurious excursion (Δ_s). The complete list of the criteria is reported in Table 2. According to these criteria, M can range between 0 and 7. Fig. 3b reports examples of measured devices with different values of M. The advantage of this metric compared to norm-based metrics is that does not require to know the spurious free-response of the resonator, which cannot be known a priori on fabricated devices.

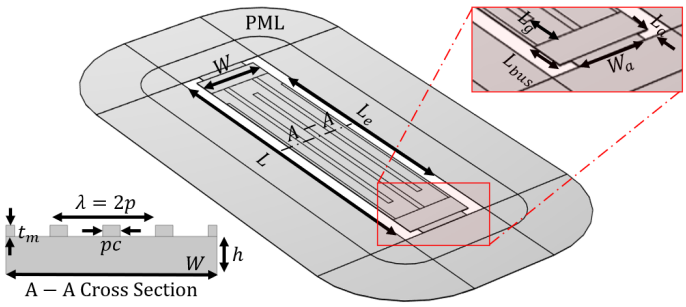

Fig. 1. COMSOL® 2D and 3D models of a LN laterally vibrating resonators. The investigated geometrical features are highlighted in the picture and consist of: 1) Acoustic wavelength (λ); 2) Number of electrode (IDEs) pairs (N_p); 3) Electrode length (L_e); 4) Finger-to-bus gap (L_g); 5) Bus length (L_b); 6) Anchor width (W_a); 7) Film thickness (h); and 8) Electrode coverage (c). Boundary conditions are set via Perfectly Matched Layers (PML).

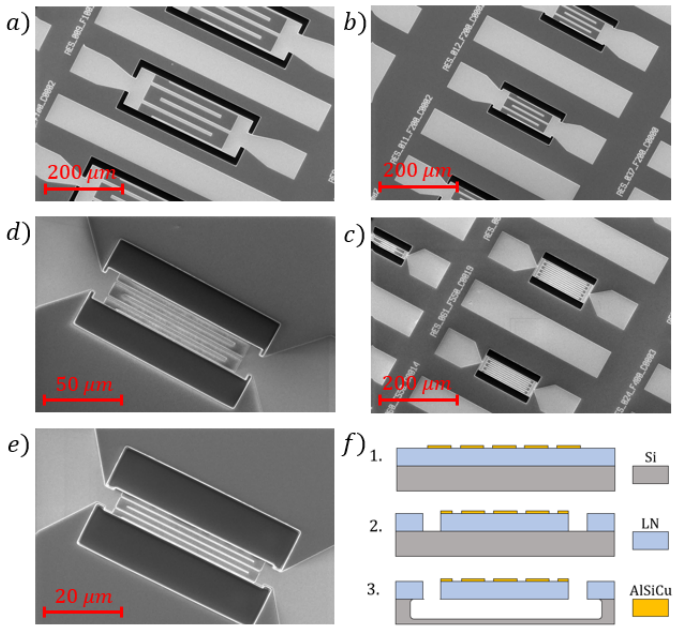

Fig. 2. SEM images of fabricated devices operating at: a) 100 MHz; b) 200 MHz; c) 400 MHz; d) 550 MHz; e) 1 GHz; and f) LN resonators fabrication process [3]: (1) Sputtering and etching of 300 nm of AlSiCu to define the top electrode; (2) Ion milling of the piezoelectric layer; and (3) Isotropic XeF_2 release.

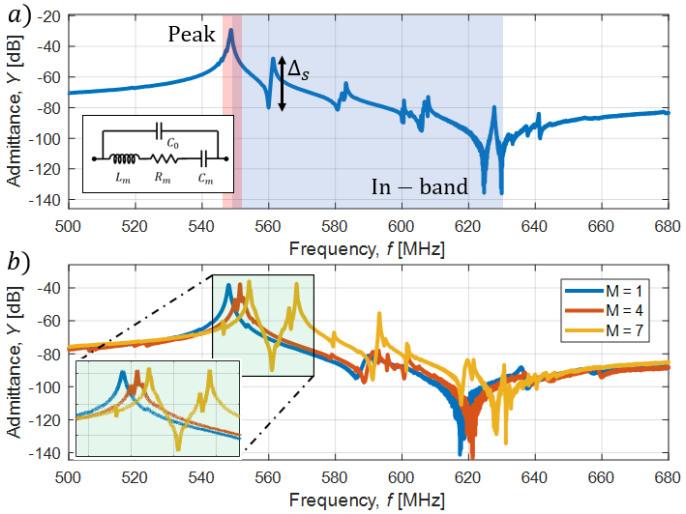

Fig. 3. a) Example of a measured LN MEMS resonator Y response. Peak and in-band regions are highlighted together with the maximum spurious peak-to-peak excursion (Δ_s). The equivalent electrical Butterworth-Van Dyke (BVD) model of a resonator is reported in the inset; and b) Example of device with different spurious modes M as defined in Table 2 and inset of the peak region.

III. Neural Network for DFS

NNs are powerful and universal analysis tools, able to learn and represent an unknown function binding certain inputs with certain outputs. In our case, the MEMS design parameters (listed in Table 1) are the inputs, while the qualitative metric M (defined upon response images and Table 2) is our output. Provided a correct network architecture and sufficient amount of data (the 814 fabricated resonators parameters and their labelling M), a NN can learn the mapping from the given samples, and return a value M^* for any other arbitrary input. We randomly split our dataset in training set (50%), validation set (25%), and test set (25%). In this work, we use a special kind of network architecture, implementing DFS, which also helps us to identify the inputs that most impact the metric score M.

Figure 4 depicts the architecture which granted the best results during the experiments. We tried different configurations, and the network with the fully connected layer of 40 nodes provided the best scores. In a DFS network, we distinguish the network parameters (also known as weights) between the ones weighting the sparse one-to-one linear layer $(w_1, \ldots, w_{10})$, and all the others (indicated with P in the following).

The DFS approach trains the NN minimizing the Mean Square Error (MSE) of the returned value M^* with the supervised value M, while at the same time regularizing the weights.

$$\min_{w,P} \sum_{i=1}^{N} \| M_i^* - M_i \|_2 + \lambda \| P \|_2 + \alpha \| w \| \qquad (1)$$

As shown in Eq. (1), the training minimizes the error on the sample data ($i = 1, \ldots, N$) while giving penalties for solutions with great weight values. This technique is commonly referred to as *regularization*, and it is usually employed to combat overfitting. In this case, however, given the particular structure of our NN, the regularization on w forces the training to pick the features that have higher chances to determine the correct value. When $\alpha = 0$, the regularization is off and the parameters can freely be used in the network; when $\alpha > 0$ the minimization is forced to trade off some feature contribution for obtaining a better score. Varying α we can hence obtain a ranking among features at different regularization levels. To regularize w we use a L_1 norm, which is more likely to grant sparsity of regularization. We also regularize with a different hyper-parameter, λ, the other NN weights, to avoid the swelling of P as α increases.

Figure 5 shows the normalized moving average of the weights w after training 1000 epochs of training as a function of α. We found 1000 epochs to be sufficient for our NN and our dataset to converge in training accuracy. We collect the values of w and we normalize them with respect to the largest to obtain a representation of their relative impact. Then we compute a moving average with memory 0.95 to better highlight the trend of the feature weight.

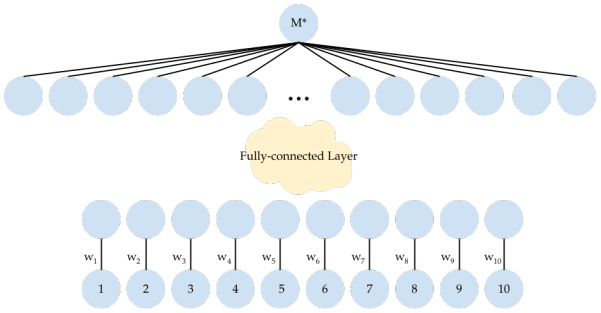

Fig. 4. Neural network architecture employed. The one-to-one layer allows the regularization of the NN parameters associated with the input features through the hyper-parameter α.

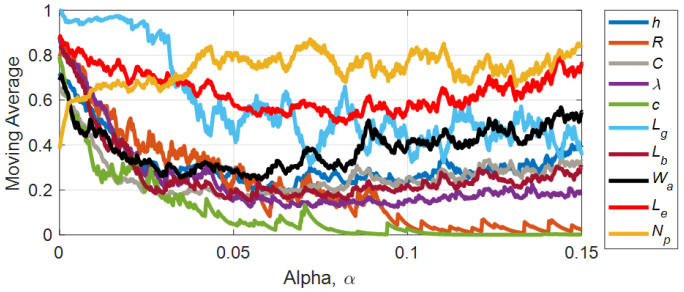

Fig. 5. Moving average (with memory 0.95) of the parameters of the one-to-one layer as a function of the regularization parameter α. Values are normalized with respect to the largest parameter.

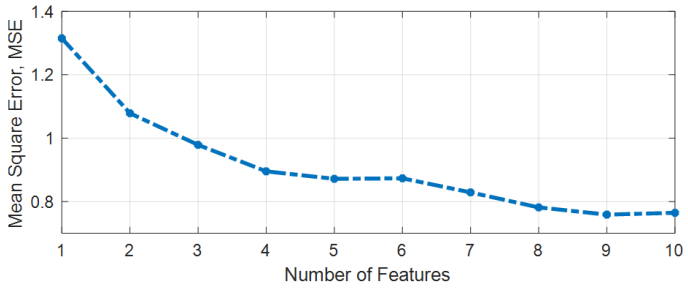

Fig. 6. Mean Square Error (MSE) on the test set as a function of the number of selected features according to the rank reported in Table 1.

The ranking result from Fig. 5 is reported in the last column of Table 2. To further highlight the different impacts that the features have in determining M, we also create and train other 9 NNs, with identical structure than the one in Fig. 4, but having only 1 to 9 inputs. For each network with n inputs, we train it with the first n features according to the ranking of Table 2. Averaged over 10 different training, the accuracy results on the test set are presented in Fig. 6. Results show how using just the first feature, N_p we obtain a MSE of just 1.3 on M. Using the first 4 features is sufficient to reach an accuracy on the test set of 0.9.

IV. Experimental Results and Model Validation

The NN detects that three features (N_p, L_e, and W_a) contributed the most to M (Fig. 5) and its mean square error (MSE, Fig. 6). This can be physically explained by the fact that wider, fully-anchored short resonator provide a path for

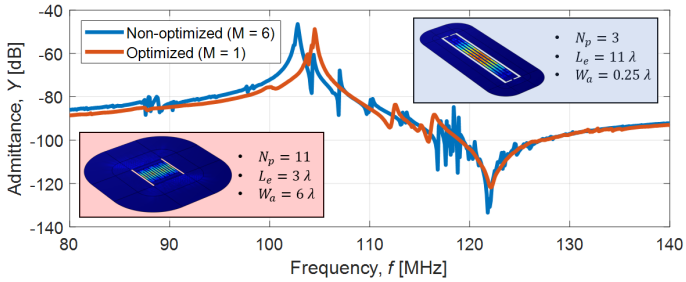

Fig. 7. COMSOL® 3D simulations of a device with optimized significant features as predicted by the NN (N_p, L_e, and W_a) versus a non-optimized device. Both the number of in-band spurious and their excursion are significantly reduced. Fixed parameters: λ = 56 μm, h = 1 mum, L_g = L_b = 0.75 λ, W_a = 0.75 λ, and c = 0.3.

the acoustic energy to escape through the substrate rather than being reflected to excite unwanted modes of vibration [20]. It also predicts that the sole device geometry is responsible for the insurgency of spurious modes, since the position-related variables (chip rows and columns) yield scarce impact on the overall MSE. Ultimately, it is demonstrated the wavelength (λ) has limited impact as well on M, hinting to the fact that spurious modes rise is a frequency-independent phenomenon.

To verify all of the hypothesis formulated according to the NN outputs, two devices with optimized and non-optimized set of features are simulated with FEA. The resonators (Fig. 7) are designed to approximately account for the same occupied area and static capacitance (C_0). According to the results reported in Fig. 7, the optimized device showcase a sensibly lower spurious modes presence (M = 1) compared to the non-optimized geometry (M = 6), validating the NN outputs.

V. Conclusions

In this paper, a NN DFS algorithm is implemented to identify the main geometrical features impacting the rise of spurious modes in sub-GHz LN resonators. A specifically designed metric (M) is introduced to evaluate the severity of in-band unwanted modes. According to the presented results, the NN succeeds in identifying the most relevant features impacting the spurious modes, thus providing useful insights for the design of high-performance devices. This analysis could be further refined by the development of a more accurate metric that discriminates between the different applications in which these resonators are implemented. Finally, this technique can be generalized to investigate the feature impact on other MEMS performance, such as Q_s and k_t^2.

Acknowledgment

This work was supported by Defense Advanced Research Project Agency Microsystems Technology Office (DARPA MTO) under the NZERO Project (contract: HR0011-15-C-0137). The authors would like to thank the staff of the Claire & John Bertucci Nanotechnology Laboratory at Carnegie Mellon University for their help and support.

References

[1] R. Ruby, "A snapshot in time: The future in filters for cell phones," *IEEE Microwave Magazine*, vol. 16, no. 7, pp. 46–59, Aug 2015.

[2] Y. Yang, R. Lu, L. Gao, and S. Gong, "4.5 GHz Lithium Niobate MEMS Filters with 10Microelectromechanical Systems, vol. 28, no. 4, pp. 575–577, Aug 2019.

[3] L. Colombo, A. Kochhar, G. Vidal-Alvarez, and G. Piazza, "High Figure of Merit X-cut Lithium Niobate MEMS Resonators Operating Around 50 MHz for Large Passive Voltage Amplification in Radio Frequency Applications," *IEEE Transactions on Ultrasonics, Ferroelectrics, and Frequency Control*, pp. 1–1, Feb 2020.

[4] M. Kadota and S. Tanaka, "Improved quality factor of Hetero Acoustic Layer (HAL) SAW resonator combining LiTaO3 thin plate and quartz substrate," in *2017 IEEE International Ultrasonics Symposium (IUS)*. IEEE, Sep 2017, pp. 1–1. [Online]. Available: http://ieeexplore.ieee.org/document/8092963/

[5] A. Lozzi, E. Ting-Ta Yen, P. Muralt, and L. G. Villanueva, "$Al_{0.83}Sc_{0.17}N$ Contour-Mode Resonators With Electromechanical Coupling in Excess of 4.5%," *IEEE Transactions on Ultrasonics, Ferroelectrics, and Frequency Control*, vol. 66, no. 1, pp. 146–153, Jan 2019. [Online]. Available: https://ieeexplore.ieee.org/document/8540088/

[6] S. Shao, Z. Luo, and T. Wu, "High Figure-of-Merit Lamb Wave Resonators Based on Al0.7Sc0.3N Thin Film," *IEEE Electron Device Letters*, vol. 42, no. 9, pp. 1378–1381, 2021.

[7] C. Cassella, Y. Hui, Z. Qian, G. Hummel, and M. Rinaldi, "Aluminum Nitride Cross-Sectional Lamé Mode Resonators," *Journal of Microelectromechanical Systems*, vol. 25, no. 2, pp. 275–285, Apr 2016. [Online]. Available: http://ieeexplore.ieee.org/document/7377005/

[8] S. S. Bedair, J. S. Pulskamp, R. Rudy, R. Polcawich, R. Cable, and L. Griffin, "Boosting MEMS Piezoelectric Transformer Figures of Merit via Architecture Optimization," *IEEE Electron Device Letters*, vol. 39, no. 3, pp. 428–431, Mar 2018. [Online]. Available: http://ieeexplore.ieee.org/document/8274910/

[9] M. E. Galanko, S. S. Bedair, R. Rudy, V. F.-G. Tseng, J. S. Pulskamp, and I. Kierzewski, "AT-Cut Quartz Piezoelectric Transformers for Passive Voltage Gain in an RF Front-End," *IEEE Electron Device Letters*, vol. 40, no. 10, pp. 1670–1673, Aug 2019.

[10] R. Wang, S. A. Bhave, and K. Bhattacharjee, "High kt²×Q, multi-frequency lithium niobate resonators," in *2013 IEEE 26th International Conference on Micro Electro Mechanical Systems (MEMS)*. IEEE, jan 2013, pp. 165–168. [Online]. Available: http://ieeexplore.ieee.org/document/6474203/

[11] R. Lu, T. Manzaneque, Y. Yang, and S. Gong, "Exploiting parallelism in resonators for large voltage gain in low power wake up radio front ends," in *2018 IEEE Micro Electro Mechanical Systems (MEMS)*. IEEE, Jan 2018, pp. 747–750. [Online]. Available: https://ieeexplore.ieee.org/document/8346663/

[12] M. Faizan and L. G. Villanueva, "Frequency-scalable fabrication process flow for lithium niobate based Lamb wave resonators," *Journal of Micromechanics and Microengineering*, vol. 30, no. 1, p. 015008, Dec 2019. [Online]. Available: https://iopscience.iop.org/article/10.1088/1361-6439/ab5b7b https://iopscience.iop.org/article/10.1088/1361-6439/ab5b7b/meta

[13] R. Lu and S. Gong, "RF acoustic microsystems based on suspended lithium niobate thin films: advances and outlook," *Journal of Micromechanics and Microengineering*, vol. 31, no. 11, p. 114001, Sep 2021.

[14] L. Colombo, M. E. Galanko Klemash, T. M. Kiebala, S. S. Bedair, G. Piazza, and M. Rinaldi, "VHF and UHF Lithium Niobate MEMS Resonators Exceeding 30 dB of Passive Gain," *IEEE Electron Device Letters*, 2021.

[15] Y. H. Song, R. Lu, and S. Gong, "Analysis and removal of spurious response in SH0 lithium niobate MEMS resonators," *IEEE Transactions on Electron Devices*, vol. 63, no. 5, pp. 2066–2073, May 2016.

[16] C. Xu, E. Calayir, G. Piazza, M. Li, and S. Zhao, "Fast and accurate prediction of spurious modes in aluminum nitride MEMS resonators using artificial neural network algorithm," *IEEE International Ultrasonics Symposium, IUS*, Oct 2017.

[17] Y. Li, C.-Y. Chen, and W. W. Wasserman, "Deep Feature Selection: Theory and Application to Identify Enhancers and Promoters," in *Research in Computational Molecular Biology*, T. M. Przytycka, Ed. Cham: Springer International Publishing, 2015, pp. 205–217.

[18] S. Rahimi, S. Mottahedi, and X. Liu, "The geography of taste: Using yelp to study urban culture," *ISPRS International Journal of Geo-Information*, vol. 7, no. 9, 2018. [Online]. Available: https://www.mdpi.com/2220-9964/7/9/376

[19] R. Zhao, P. J. Kollmeyer, R. D. Lorenz, and T. M. Jahns, "A compact methodology via a recurrent neural network for accurate equivalent circuit type modeling of lithium-ion batteries," *IEEE Transactions on Industry Applications*, vol. 55, no. 2, pp. 1922–1931, 2018.

[20] J. Segovia-Fernandez and G. Piazza, "Analytical and Numerical Methods to Model Anchor Losses in 65-MHz AlN Contour Mode Resonators," *Journal of Microelectromechanical Systems*, vol. 25, no. 3, pp. 459–468, Jun 2016. [Online]. Available: http://ieeexplore.ieee.org/document/7438751/